journal of the mechanical behavior of biomedical materials 148 (2023) 106186

Contents lists available at ScienceDirect

Journal of the Mechanical Behavior of Biomedical Materials

journal homepage: www.elsevier.com/locate/jmbbm

Research paper

Scaphoid numerical simulation of the critical loading until fracture

Ana B. Maroto [a,b], Pedro Navas [a,*], Felicia Alfano [b,c]

[a] Continuum Mechanics and Theory of Structures Dep. Civil Eng. School, Universidad Politécnica de Madrid, Prof. Aranguren 3, 28040, Madrid, Spain
[b] Biomedical Image Technologies, Universidad Politécnica de Madrid, Av. Complutense, 30, 28040, Madrid, Spain
[c] CIBER-BBN, ISCIII, Av. Monforte de Lemos, 3-5, 28029, Madrid, Spain

ARTICLE INFO

Keywords:
Finite Element Analysis
Biomechanics
Bone damage
Computerized Tomography

ABSTRACT

The numerical study of the scaphoid fracture, although it is relatively unexplored, can be of great clinical interest since it is highly common and can result in temporary or persistent disability.

In this manuscript, seven combinations of boundary conditions and contacts between adjacent bones, together with four different loads, simulating real hand movements, are assessed.

Three different fracture criteria for bones are employed to study the failure of the scaphoid with the aforementioned combination of interaction conditions. The results offer an interesting view of the accuracy of the possible interaction between adjacent bones. For future calculation, it would be possible to choose a combination of the balance between precision and computational cost savings.

This study provides a comprehensive assessment into the modeling of the scaphoid bone and its interactions with adjacent bones. The findings reveal that various choices of interactions can yield similar results, allowing for flexibility in selecting interaction models based on desired accuracy or computational efficiency. Ultimately, this study establishes a foundational understanding for future research on modeling scaphoid motion.

1. Introduction

Wrist bones exhibit a heightened susceptibility to fracture due to their vulnerability to trauma and various impacts, regardless of the individual's age. However, it has also been observed that bone mechanical properties undergo substantial alterations with age, leading to a diminished capacity to withstand loading forces and subsequently lowering their resistance (Keyak et al., 2013).

The fracture of the scaphoid bone is highly common and can result in temporary or persistent disability. Therefore, the study of this relatively unexplored bone fracture can be of great clinical interest. The utilization of numerical models based on the finite element method enables the assessment of bone's mechanical behavior, taking into account its elastic range and fracture initiation. This approach contributes to provide deeper insights into bone behavior, thereby benefiting the fields of biomechanics and clinical practice.

The main goal of Finite Element Analysis (FEA) of scaphoid fracture is to provide a quantitative and accurate understanding of the mechanical behavior of the scaphoid bone under different loading conditions, and to evaluate the effectiveness of various treatment methods for scaphoid fractures. FEA is a computer-based method that uses mathematical modeling and simulation techniques to predict the mechanical response of a structure to various loads and boundary conditions. In the case of scaphoid fracture, FEA can be used to investigate the effects of different factors, such as the size and location of the fracture, the orientation and position of the implant, and the biomechanical properties of the bone and surrounding tissues. This information can be used to optimize treatment strategies and improve clinical outcomes for patients with scaphoid fractures.

A thorough understanding of bone fracture patterns in any bone is still a challenge and an active field of research. In this context, computational models, together with experimental validations, are an indispensable tool for fracture behavior prediction because of their complementary nature (Cristofolini et al., 2010; Enns-Bray et al., 2016). An interesting review of the parameters, behavior and fracture of the scaphoid can be found in Tortora and Derrickson (2018). Additionally, a comprehensive review specifically focused on scaphoid bone was conducted by Slutsky and Slade (2011). Numerous studies on bone fractures rely solely on imaging of the fractured material. However, it is widely acknowledged that the accuracy of such results is not as precise as those obtained through the utilization of numerical modeling techniques (Falcinelli et al., 2016; Cody et al., 1999). Although there is a scarcity of finite element studies of the scaphoid, in this preliminary research, we aim to establish the basis of a comprehensive analysis of the factors contributing to the scaphoid's fracture using different criteria.

The current state of the art for FEA of scaphoid fracture is limited. Varga et al. (2016) presented an analysis for screw design as well as

* Corresponding author.
E-mail address: pedro.navas@upm.es (P. Navas).

https://doi.org/10.1016/j.jmbbm.2023.106186
Received 10 July 2023; Received in revised form 4 October 2023; Accepted 10 October 2023
Available online 14 October 2023

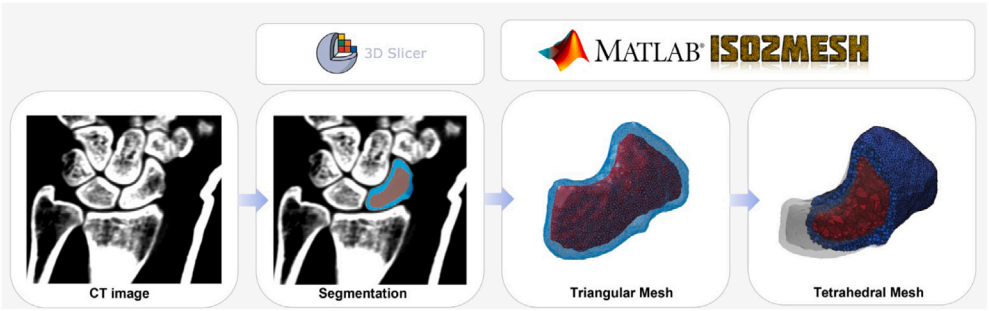

Fig. 1. Workflow of employed software.

Luria et al. (2010) studied the optimal fixation; Bajuri et al. (2012) analyzed the effects of rheumatoid arthritis; and, more recently, Rothenfluh et al. (2023) examined the impact of partial union on the strength of the scaphoid bone. The main purpose of this research is to investigate the impact of different movements of the wrist on the possibility of fractures, as well as the forces required to induce them. In this research, various fracture criteria will be evaluated without initiating the fracture process. The study aims to identify several locations that are most susceptible to crack initiation.

About the available fracture criteria, Doblaré and coworkers (Doblaré et al., 2004) proposed an interesting analysis of the different possibilities to model the initiation of the fracture in bones. It can be summarized as follows:

- Von Mises Criterion (also known as Hencky criterion): This criterion is not considered highly realistic for bone tissue, since it assumes equal strength in tension and compression. However, it has been widely used to estimate proximal femoral fracture loads and assess hip fracture risk. Interesting when only tension or compression failure is assessed.
- Hoffman Criterion: accounts for different strengths in tension and compression, but assumes the same behavior in all directions. It has been used to predict fractures, improving the previous one when the behavior of the anisotropic constituent of the bone takes place (mainly the trabecular part). Thus, it can be considered an extension of the previous one (in fact, they are the same if tension and compression limits coincides), being both successfully employed in bone fracture mechanics (Keyak and Rossi, 1983; Lotz et al., 1991; Fenech and Keaveny, 1999).
- Rankine or Maximum Stress Criterion: Originally designed for brittle materials, it predicts failure when the highest principal stress exceeds the ultimate strength in tension or compression. It has been used to predict bone fracture with a 30% of error. If this method is employed through strains rather than stresses, it is called Saint–Venant Criterion, reducing the error since it fits better with experiments. The high reported error made us to avoid this method.
- Mohr–Coulomb Criterion: Commonly used for materials with different tension–compression behavior, it has been applied to bone tissue with good agreement when certain conditions are met. Generally, the results are on the safety side, that is, the predicted fracture loads are always lower than the experimental ones. Thus, it has been neglected.
- Tsai–Wu Quadratic Criterion: An anisotropic failure criterion that considers strength asymmetry and anisotropy. It has been used with varying degrees of success for predicting bone fractures (Keaveny et al., 1999), but it requires multiple experimental tests to determine constants, information that is not provided for the proposed cases.
- Cowin's Fracture Criterion: This criterion is designed for porous materials and composites, taking into account porosity and fabric tensor. It has been cited but not widely used in computational simulations due to the difficulty of determining all the parameters involved. In order to simplify this methodology, Cowin (1986) gives some indications to determine the constants from the ultimate strengths of the material in the different directions and orientations. Thus, the method employed in this manuscript is the simplification of this methodology.
- Pietruszczak's Criterion: This criterion considers the stress state, fabric tensor, and porosity and has been applied to bone tissue to predict fractures. As well as the Tsai–Wu Quadratic criterion, we could not get information of the fabric tensor and the quality of images cannot provide porosity data.

After this introduction, the paper is organized as follows. Section 2 shows the methodology of the study, describing the image treatment and the finite element model, as well as the employed fracture criteria. The assessment of the results is made in Section 3 and, finally, conclusions and the discussion of the results are provided in Section 4.

2. Methodology

Following, the computational tools as well as the numerical hypotheses are described.

First, medical image processing tools have been used to perform the segmentation and meshing of the image. Specifically, `3D Slicer` and in-house `MATLAB` codes were used, respectively. Details of the image treatment are provided in Section 2.1.

Secondly, the commercial FE software Abaqus has been employed in order to carry out the numerical simulations. Every detail of the modeling of the problem is depicted in Section 2.2.

The employed tools and their workflow are shown in Fig. 1.

Finally, as mentioned before, this study aims to analyze the pre-fracture process. Indeed, this is the most interesting part since, once the failure occurs, independently of its degree of failure, the wrist loses its whole functionality. This fact makes us focus on when the fracture initiates. Thus, two components are to be assessed prior to start modeling the scaphoid behavior: the fracture criteria and the evaluation of the strength. Both are shown in Sections 2.3 and 2.4.

2.1. Image treatment

The model was obtained from a computed tomography (CT) image of a healthy wrist 2. The data covered approximately 0.332 mm × 0.332 mm × 0.300 mm real volume per voxel. CT imaging is a valuable tool that can not only detect the presence of a scaphoid fracture, but also determine whether it is a displaced fracture. Furthermore, it is also used to define treatment options.

The segmentation was carried out with the aforementioned software `3D Slicer` using thresholding and morphological filters. Both cortical and trabecular bone were segmented Fig. 2. The cortical bone (blue) was obtained as the subtraction of the segmentation of the whole scaphoid (green) and the segmentation of the trabecular bone and (red).

Fig. 2. CT image of the wrist and bones segmentation: (a) complete scaphoid, (b) trabecular bone, (c) cortical bone and trabecular bone.

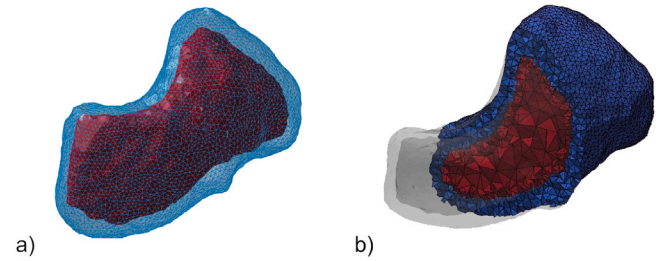

Fig. 3. (a) Triangular mesh of trabecular (red) and Cortical Bone (blue). (b) (a) Tetrahedral mesh of trabecular (red) and Cortical Bone (blue).

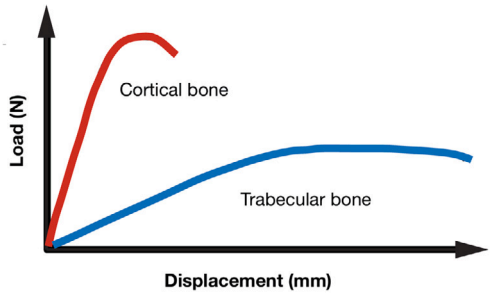

Fig. 4. Load–displacement curve of the biomechanical behavior of bone parts. *Source:* Adapted from Caeiro et al. (2013).

The segmentation was exported as 3D binary image and meshed in `MATLAB` as 3D tetrahedral finite element (FE) mesh using `iso2mesh library` (Fang, 2022). Preceding the generation of the tetrahedral mesh, we applied a smoothing filter to the surface mesh, ensuring that it did not excessively alter the bone's singularities, which are crucial for crack initiation.

A more refined mesh resolution was employed for cortical bone, characterized by its higher density and compact composition, while a comparatively coarser mesh was utilized for trabecular bone, distinguished by its porous and spongy nature.

However, the decision to refine the mesh for the cortical portion is not contingent on its intrinsic density but is instead based on the fact that the majority of the applied load energy, and consequently the stresses, are absorbed by the stiffer component, namely, the cortical bone. Consequently, any potential crack is more likely to manifest within the cortical bone. Therefore, we opted to enhance the resolution of this bone segment while employing a coarser mesh in the inner trabecular part to save computational time. The selected mesh size for the cortical part was able to properly capture any singularity of the scaphoid body.

Fig. 3 shows the tetrahedral meshes for the cortical and trabecular bones.

2.2. Finite element model

2.2.1. Formulation and constitutive model

As the result of the material properties of each of the bone components and their geometric distribution, the mechanical behavior of a bone is highly complex (Caeiro et al., 2013). As all bones in the body are not identical, their particular characteristics can also affect their behavior, such as their density, thickness or diameter.

In general terms, bones are modeled as elastic materials, since they can recover their original shape after the remission of a load.

Based on the bone's structure and biomechanical behavior, two types of tissue can be identified: cortical (or compact) bone and trabecular (or cancellous or spongy) bone. Cortical bone exhibits a higher elastic modulus, resulting in a steeper stress–strain curve (see Fig. 4). This allows it to withstand high loads per unit area with minimal deformation, making it very rigid (Caeiro et al., 2013). On the other hand, trabecular bone has a lower Young's modulus and a flatter stress–strain curve, indicating a lower load per unit area but with greater strain rate, making it more flexible (Caeiro et al., 2013).

Table 1
Mechanical properties of bone (Varga et al., 2013; Anderson et al., 2005; Villalobos, 2007).

Reference	Type of material	E (cortical)	E (trabecular)	ν
Varga et al. (2013)	Plastic (only cartilage, E=5 MPa)	–	–	0.3
Donald et al. (2005)	Isotropic linear elastic	13.8 GPa	400, 690 and 345 MPa	0.3
Pérez (2007)	Isotropic linear elastic	10 GPa	1 GPa	0.35

In this study, the scaphoid bone was modeled as a structure consisting of two parts, cortical and trabecular, each with their own distinct properties and mechanical behaviors, which were described using different materials. There has been extensive research on bone component behavior based on the density of the porous medium (Helgason et al., 2008; Schileo et al., 2008).

Isotropic elastic constitutive models were utilized to model both parts, but with different elastic parameters assigned to each. This is due to the clear discrepancy in mechanical strength between the two parts.

In order to determine the elastic constants for the model, a thorough examination was conducted on the previous usage of Young's modulus (E) and Poisson's coefficient (ν) values.

Table 1 summarizes the mechanical properties used for the scaphoid. The values of Poisson's coefficient are chosen the same for the cortical and trabecular bones (Helgason et al., 2008).

2.2.2. Boundary conditions and contact mechanics

The scaphoid bone is surrounded by the radius, capitate, lunate, trapezium and trapezoid bones.

The extent of contact area between the scaphoid and the adjacent bones varies depending on the positioning of the wrist. In order to define the regions of interest where boundary conditions need to be

Table 2
Contact areas (mm^2) between the scaphoid and neighboring bones at different positions of the wrist (Varga et al., 2013).

Bone	UN	LN	PE	TE	PF	TF	UA	RA	Avg.
Capitate	60,22	57,17	40,14	45,93	50,02	42,13	39,25	57,57	48,42
Radius	12,14	27,89	31,51	28,82	34,4	21,4	–	49,07	27,23
Trapezium	4,05	8,99	10,42	19,28	16,07	17,57	–	28,57	12,89
Lunate	0,42	–	10,07	14,45	10,48	17,47	–	13,37	7,29
Trapezoid	–	–	–	0,61	–	–	–	1,4	0,92

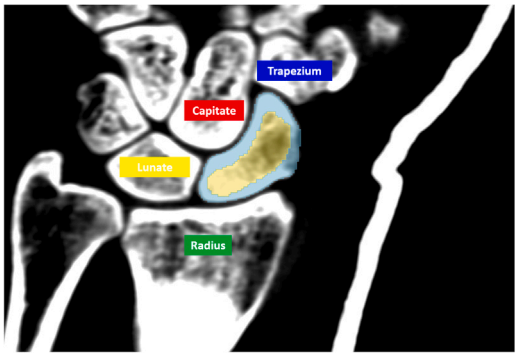

Fig. 5. Bones in contact with the scaphoid.

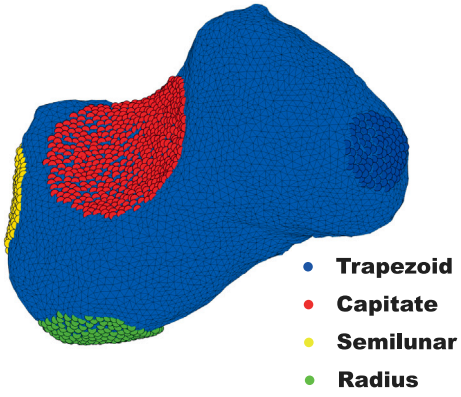

Fig. 6. Sets of nodes of each interaction with neighbor bones.

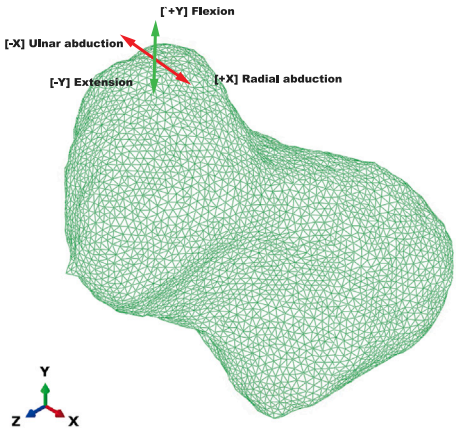

Fig. 7. Coordinate reference system.

applied, the average values of eight wrist positions (UN: neutral without load, LN: neutral load, PE: partial extension, TE: total extension, PE: partial flexion, TF: total flexion, UA: ulnar abduction, AR: radial abduction) have been calculated.

Table 2 presents the contact bones arranged in descending order based on their average contact area. The trapezoid bone is not significantly in contact with the scaphoid bone in any wrist position, as shown in the table. Therefore, this junction was disregarded.

Therefore, only the capitate, the radius, trapezium and lunate bones were considered for contact mechanics as shown in Fig. 5.

To simulate the interaction with the contact bones, a set of nodes at the interface was automatically calculated on the surface mesh of the scaphoid for each contact bone.

The nodes for each region at the interface with the contact bones were automatically selected starting from a reference point marked in the CT image using `3D Slicer`. Starting from the reference point position, the surrounding nodes for each of the regions were calculated in `MATLAB` considering surface nodes within a certain radius chosen taking into account the size of the contact surface (Table 2). The volumetric mesh and the boundary nodes were directly imported into `Abaqus` as *inp* file. Fig. 6 shows the boundary nodes for each contact region.

Based on the study by Erhart et al. (2020), the simulation examined the behavior of the scaphoid in the four main movements of the hand: flexion, extension, radial abduction and ulnar abduction.

In order to simulate flexion, extension, radial abduction, and ulnar abduction on a bone surface, it is necessary to define the direction and manner in which force is applied while ensuring that it remains perpendicular to the bone surface. In the coordinate system shown in Fig. 7, force is applied in the positive Y-axis direction (+Y) for flexion and in the negative Y-axis direction (−Y) for extension. Similarly, radial abduction is simulated by applying force in the positive X-axis direction (+X), and ulnar abduction is simulated by applying force in the negative X-axis direction (−X).

In accordance with the study on the movement pattern of the scaphoid by Erhart et al. (2020), certain assumptions were made regarding its interactions with the surrounding bones.

Specifically, the points at the interface with the radius were treated as fixed, while the interaction with the trapezium was modeled as a set of concentrated forces in the nodes of this region. However, the interactions with the capitate and the lunate were unclear. For this reason, two simulations set ups have been considered. The first one is based on Dirichlet boundary conditions imposed on the points at the interface between the scaphoid and the capitate and lunar bones, respectively. The other one is based on surface contact-type interactions between the scaphoid and both the capitate and lunar bones. The contact surfaces, were automatically generated using self-made subroutines in `MATLAB`. These surfaces were designed to simulate the external faces of the neighboring bones (Fig. 8).

The latter approach, while more computationally demanding, allows for the replication of realistic separations that may occur between the bones.

In summary, the study aimed to analyze scaphoid fractures in relation to four hand movements using different scenarios to model the interaction at the interface between the scaphoid and the surrounding bones. Table 3 provides an overview of the considered scenarios at the interface, including four combinations of Dirichlet boundary conditions (BC) and three Contact-Type Interactions (CI).

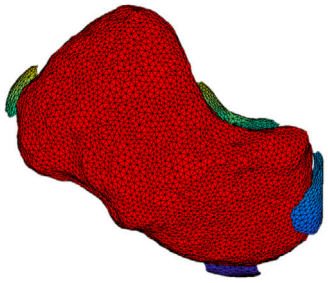

Fig. 8. Scaphoid contact surfaces.

Table 3
Combinations of boundary conditions (BC) and contact interactions (CI).

	Radius	Capitate	Lunate	Trapezium
BC I	Fixed	Free	Free	Load
BC II	Fixed	Fixed	Free	Load
BC III	Fixed	Free	Fixed	Load
BC IV	Fixed	Fixed	Fixed	Load
CI I	Fixed	Contact	Free	Load
CI II	Fixed	Free	Contact	Load
CI III	Fixed	Contact	Contact	Load

2.3. Fracture criteria

The fracture of the bone has been studied using fracture criteria focused on the study of failure under isotropic conditions, since the two constituent parts of the scaphoid, trabecular and cortical bone, have been modeled as isotropic linear elastic materials. In accordance with the information presented in Section 1, the von Mises, Hoffman, and Cowin criteria have been taken into chosen due to their prevalent usage in the field of bone mechanics. This choice stems from the limited availability of anisotropic data regarding bone behavior, which restricts the utilization of more sophisticated criteria. A wide review of these methodologies is made by Yeh et al. (2009).

2.3.1. Von Mises criterion

The von Mises criterion, also called the maximum distortion energy criterion, is used in studies of static strength and ductile materials (Frank and Von Mises, 1961). The statement asserts that at a specific point, the attainment of yield will be prevented as long as the distortion energy per unit volume remains lower than the distortion energy associated with yielding for that particular point, which can be determined through a tensile test conducted on the material (Frank and Von Mises, 1961; de Souza Neto et al., 2008).

This criterion is defined through Eq. (1), where σ_1, σ_2 and σ_3 are the principal stresses and σ_{eq} is the equivalent stress, also known as von Mises stress.

$$2\sigma_{eq}^2 = (\sigma_1 - \sigma_2)^2 + (\sigma_2 - \sigma_3)^2 + (\sigma_3 - \sigma_1)^2 \tag{1}$$

This criterion is widely recognized; however, its application assumes that the material exhibits similar behavior in both tensile and compression tests. Consequently, it may not be the most suitable criterion for studying the failure of bone tissue. However, on numerous occasions it has been used to evaluate the failure of this type of tissue, as for example in the study by Keyak et al. (2001).

The yield strength value obtained through this criterion was used to calculate the fracture risk coefficient (FR), which is defined as Oliva (2007):

$$FR = \frac{\text{Equivalent stress}}{\text{Last stress}} = \frac{\sigma_{eq}}{\sigma^+}, \tag{2}$$

where the ultimate stress is taken as the tensile strength (σ^+), in tension. Thus, failure may occur when FR is greater than the unity.

2.3.2. Hoffman criterion

According to Hoffman's criterion, also known as the maximum normal stress criterion, bone failure occurs when the maximum normal stress, either tensile or compressive, surpasses the strength limit of the bone. This criterion assumes that failure is primarily driven by the maximum stress acting on the bone rather than considering other factors such as stress concentration, strain rate, or the presence of microcracks.

Contrary to the previous one, Hoffman's criterion (Hoffman, 1967) does consider the distinction between tensile and compressive strengths, so it is expressed in terms of principal stresses (σ_1, σ_2 and σ_3), tensile strength (σ^+) and compressive strength (σ^-). It states that bone will fracture when the maximum normal stress at a critical location exceeds the ultimate tensile strength of the bone material (Oliva, 2007):

$$\begin{aligned}\left[\frac{1}{\sigma^+} - \frac{1}{\sigma^-}\right](\sigma_1 + \sigma_2 + \sigma_3) + \left[\frac{1}{\sigma^+ \cdot \sigma^-}\right](\sigma_1^2 + \sigma_2^2 + \sigma_3^2) + \\ + \left[-\frac{1}{\sigma^+ \cdot \sigma^-}\right](\sigma_1\sigma_2 + \sigma_1\sigma_3 + \sigma_2\sigma_3) = 1\end{aligned} \tag{3}$$

2.3.3. Cowin criterion

Cowin (1986), based on the methodology of Malmeister (1966) and Tsai and Wu (1971), proposed a tissue structure-dependent breakage criterion (Oliva, 2007). This criterion considers the fabric, which refers to the orientation distribution of collagen fibers within the bone matrix, as a key factor influencing the mechanical behavior and strength of bone. The fabric-dependent criterion suggests that bone will fail when the stress tensor exceeds a critical value that is determined by the fabric orientation.

The specific mathematical formulation and details of Cowin's criterion may vary depending on the particular study. The formulation of this criterion for the case of an isotropic material is defined according to the following equation:

$$\begin{aligned}G_{11}(\sigma_1 + \sigma_2 + \sigma_3) + \\ + F_{1111}(\sigma_1^2 + \sigma_2^2 + \sigma_3^2) + \\ + 2F_{1122}(\sigma_1\sigma_2 + \sigma_1\sigma_3 + \sigma_2\sigma_3) = 1\end{aligned} \tag{4}$$

In Eq. (4), σ_i are the principal stresses and G_{11}, F_{1111} and F_{1122} are parameters whose value is given by the tensile, compressive and tangential strengths as follows:

$$G_{11} = \frac{1}{\sigma^+} - \frac{1}{\sigma^-} \tag{5}$$

$$F_{1111} = \frac{1}{\sigma^+\sigma^-} \tag{6}$$

$$F_{1122} = \frac{1}{\sigma^+\sigma^-} - \frac{1}{2\tau^2} \tag{7}$$

2.4. Tensile, compressive and tangential strength

Tensile strength (σ^+), compressive strength (σ^-) and tangential strength (τ) are characteristic values of each material that allow the evaluation of its mechanical behavior.

While analyzing scaphoid fractures, the bone has traditionally been conceptualized as consisting of two components, namely cortical and trabecular. However, in the assessment of fractures using the aforementioned criteria, only the comparative strengths of the cortical bone have been considered. This is primarily due to its direct interaction with the neighboring carpal bones, thus experiencing different forces, as well as the aforementioned boundary condition actions. Moreover, the cortical bone, characterized by a higher elastic constant (E), is significantly more influenced by stress-related actions than the inner part, with lower Young's modulus.

According to Gómez-Benito et al. (2007), compressive strength (σ^-) depends on strength, density and an experimental parameter that takes values between 1 and 2 MPa. It can be calculated through:

$$\sigma^- = \sigma_0^- \left(\frac{\rho}{\rho_0}\right)^\gamma \tag{8}$$

In Eq. (8), the reference values are set to $\sigma_0^- = 15.8$ MPa, $\rho_0 = 0.45$ g/cm^3 and the parameter $\gamma = 1.8$ (Oliva, 2007).

The tensile strength (σ^+) is defined as a fraction of the compressive strength (Oliva, 2007). This ratio is defined by the parameter *alpha* which takes values between 0.4 and 0.6 and, in this case, the average value 0.5 (Oliva, 2007) has been used. The calculation of the resistance in tensile tests is given by the following formula (Oliva, 2007):

$$\sigma^+ = \alpha \cdot \sigma^- \tag{9}$$

The resistance to tangential stresses is expressed as follows (Oliva, 2007):

$$\tau = \tau_0 \left(\frac{\rho}{\rho_0} \right)^{\gamma} \tag{10}$$

where $\tau_0 = 69$ MPa, $\rho_0 = 1.92$ g/cm^3 and $\gamma = 1.4$ are taken as reference values (Oliva, 2007).

Considering a cortical bone density equal to 1.92 g/cm^3 (Oliva, 2007), the values corresponding to each of the strengths, which agree with the values obtained by Caeiro et al. (2013), are as follows:

$$\sigma^- = 15.8 \left(\frac{1.90}{0.45} \right)^{1.8} \simeq 211 \text{ MPa} \tag{11}$$

$$\sigma^+ = 0.5 \cdot 211 \simeq 106 \text{ MPa} \tag{12}$$

$$\tau = 69 \left(\frac{1.90}{1.92} \right)^{1.4} \simeq 68 \text{ MPa} \tag{13}$$

Based on the obtained strength values and the aforementioned fracture criteria, the assessment of scaphoid fractures can be conducted in the designed models. In this context, if the resulting value is equal to or greater than 1, it indicates a prediction of fracture occurrence.

3. Results of the scaphoid fracture simulation

The main objective of this work, and thus, of this section, is to obtain an estimate of the loads that cause scaphoid fracture under different boundary conditions and with different load configurations.

The model taken as a reference consists of the two constituent parts (cortical on the outside and trabecular on the inside) of the scaphoid bone. Taking into account the mechanical properties of the bone (Table 1), an isotropic elastic material with $E = 10$ GPa and $\nu = 0.35$ has been created to define the cortical bone, while the same type of material has been used for the trabecular bone, but with $E = 1$ GPa and $\nu = 0.35$.

We took as a starting point the value of the force used in the study by Luria et al. (2010) on the optimal fixation of acute scaphoid fractures. It was tested whether, for a total force of 212 N applied on the set of nodes (100 nodes) located in the region in contact with the trapezium, trauma occurred.

From this model, as a first approximation, direct boundary conditions have been studied and then, deepening in a more sophisticated model, the contacts with neighboring bones have been considered. This study has been made with a mesh of 74685 elements and an average mesh size of 1.85 mm. In order to assess the suitability of this mesh, a convergence study is presented in the last Section, 3.3.

3.1. Direct boundary conditions

First, only one fixation has been imposed in the area of the scaphoid that articulates with the radius, as well as the aforementioned load. The interaction with the radius is expected to be the most rigid one. This combination of conditions is called *Boundary Conditions I*. Their results are depicted in Table 4 for the 4 possible movements, explained in Section 2.2.2. It is observed that the fracture may occur (except for Cowin criterion) in flexion and extension, (Y direction), but not in X direction.

Table 4
Fracture criteria with 212 N load and boundary conditions (I).

Movement	Direction	FR	Hoffman	Cowin
Flexion	+Y	1.53	1.98	0.02
Extension	−Y	1.52	3.44	0.44
Radial abduction	+X	0.55	0.61	0.3
Ulnar abduction	−X	0.55	0.79	0.42

Table 5
Fracture criteria with 212 N load and boundary conditions (II).

Movement	Direction	FR	Hoffman	Cowin
Flexion	+Y	0.1	0.002	0.001
Extension	−Y	0.1	0,009	0.007
Radial abduction	+X	0.22	0.02	0.01
Ulnar abduction	−X	0.22	0.46	0.24

Table 6
Fracture criteria with 212 N load and boundary conditions (III).

Movement	Direction	FR	Hoffman	Cowin
Flexion	+Y	0.15	0.18	0.15
Extension	−Y	0.15	0.03	0.02
Radial abduction	+X	0.25	0.21	0.22
Ulnar abduction	−X	0.25	0.16	0.13

Table 7
Fracture criteria with 212 N load and boundary conditions (IV).

Movement	Direction	FR	Hoffman	Cowin
Flexion	+Y	0.09	0.001	0.002
Extension	−Y	0.09	0.01	0.01
Radial abduction	+X	0.09	0.003	0.003
Ulnar abduction	−X	0.21	0.42	0.14

Secondly, based on the previous model, an additional fixation has been imposed in the area of the scaphoid close to the large bone, in contact with the capitate bone. This combination of conditions is called *Boundary Conditions II*. Results are shown in Table 5, observing a very low risk of failure since there is a very constrained movement.

Thirdly, the fixation in the region of articulation with the radius has been maintained, and a new one has been added in the region of union with the lunate. This combination of conditions is called *Boundary Conditions III*. In this case, the risk grows in the X movements, radial and ulnar abductions, but far from the fracture (see Table 6 for details).

Finally, a combination of the second and third applied boundary conditions has been performed. Therefore, the movement of the scaphoid has been limited in all its junction areas with the neighboring bones. This combination of conditions is called *Boundary Conditions IV*. Again, the lunate fixation makes difficult the movement of the whole bone, and thus, any risk of failure, as it is seen in Table 7.

Taking into account the results obtained, we can conclude that, for a load of 212 N, the scaphoid is susceptible to breakage only if such force has been applied in the direction of the Y axis in either direction (positive and negative) and with the only fixation in the radius, not interacting with the rest of the bones in the wrist joint.

As can be seen in Figs. 9(a), 9(b), 9(c) and 9(d), for both flexion and extension movements, the fracture occurs at the proximal pole of the scaphoid and, more specifically, in the region close to the articulation with the radius, in which region the piece is fixed. It is necessary to remember that, these figures are depicted for the set of *Boundary Conditions I*.

If we focus on the type of applied force, the ones in X direction are shear force and the ones in Y, tension (flexion) and compression (extension). From this interpretation, we can infer that Cowin criterion works similarly than the two other criteria in shear, but not in tension/compression, which is totally different. Indeed, one of the arguments of Cowin criterion is the tangential strength. Thus, for shear,

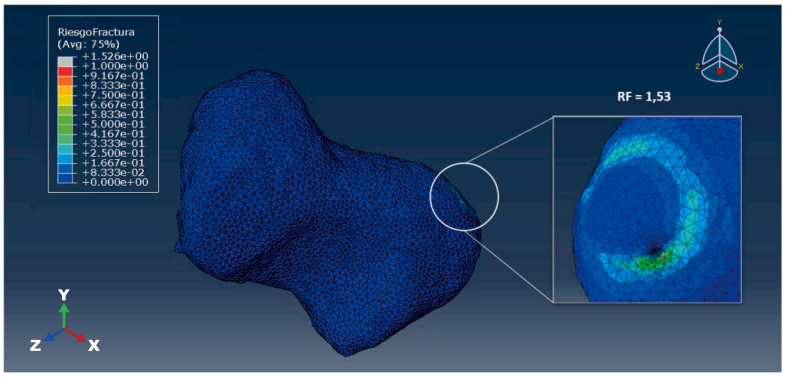

(a) Fracture risk: 212 N, flexion (I).

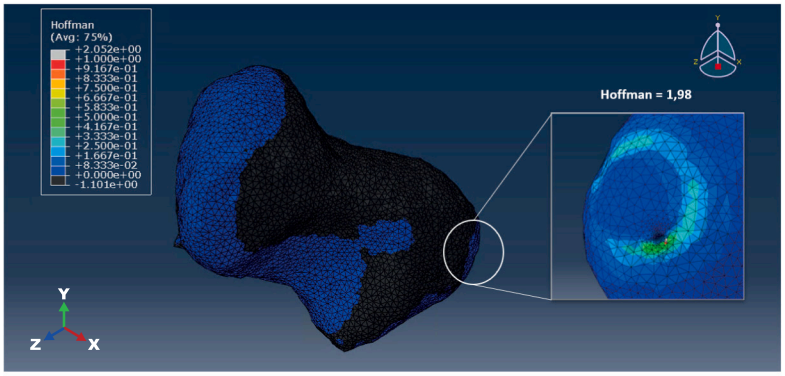

(b) Hoffman Criterion: 212 N, flexion (I).

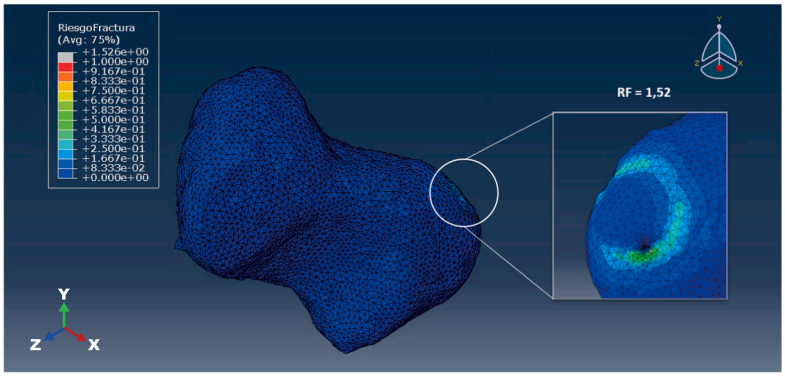

(c) Fracture risk: 212 N, extension (I).

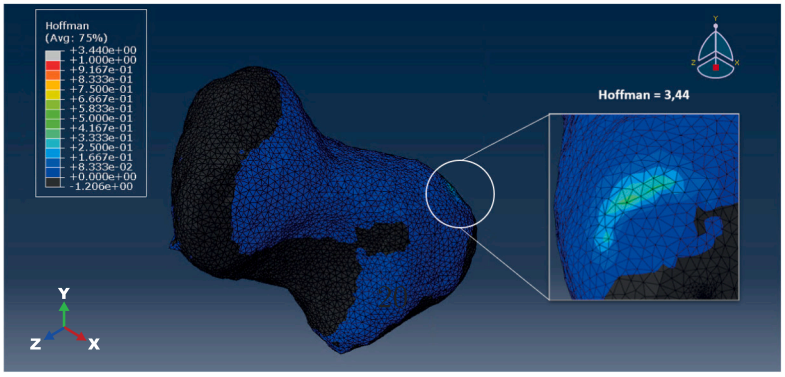

(d) Hoffman Criterion: 212 N, extension (I).

Fig. 9. Location of possible fracture for flexion and extension (Hoffman criterion and Fracture risk).

Table 8
Critical strength with boundary conditions (I).

Movement	Strength	FR	Hoffman	Cowin
Flexion	110 N (+Y)	0.77	**1.00**	–
Extension	60 N (−Y)	0.44	**1.00**	–
Radial abduction	300 N (+X)	0.52	**1.00**	0.32
Ulnar abduction	200 N (−X)	0.66	**1.00**	0.58

Table 9
Critical strength with boundary conditions (II).

Movement	Strength	FR	Hoffman	Cowin
Flexion	2100 N (+Y)	**1.01**	0.75	–
Extension	1000 N (−Y)	0.48	**1.03**	–
Radial abduction	950 N (+X)	**1.003**	0.02	0.01
Ulnar abduction	430 N (−X)	0.46	**1.00**	0.16

Table 10
Critical strength with boundary conditions (III).

Movement	Strength	FR	Hoffman	Cowin
Flexion	1000 N (+Y)	0.52	**1.04**	–
Extension	1650 N (−Y)	**1.01**	0.87	–
Radial abduction	580 N (+X)	0.69	**1.00**	0.58
Ulnar abduction	840 N (−X)	**1.00**	0.98	0.90

Table 11
Critical strength with boundary conditions (IV).

Movement	Strength	FR	Hoffman	Cowin
Flexion	2200 N (+Y)	**0.99**	0.78	–
Extension	1100 N (−Y)	0.49	**1.03**	–
Radial abduction	2150 N (+X)	**1.00**	0.74	0.58
Ulnar abduction	450 N (−X)	0.45	**0.99**	0.19

it can be more accurate than the rest of the criteria, but it is not working properly on tension/compression.

Once the response of the model when subjected to a load of 212 N was known, a search for the load to be applied to achieve fracture in each of the configurations was carried out. The strength will be the first to achieve a fracture ratio of 1 in any of the 3 criteria for shear (X) and FR and Hoffman for tension/compression (Y). In the following tables, the chosen fracture criterion is marked in bold.

In the first place, it was previously found that a load of 212 N applied in the *Y*-axis direction already caused fracture. Thus, we look for a lower value of the exerted load, the one that may break the bone. However, to achieve fracture in the *X*-axis direction, higher loads have to be applied (see Table 8). Regardless of the value and direction of the force, for this configuration, fracture always occurs at the proximal pole of the scaphoid.

For the second set, *boundary conditions II*, an increase of the load, compared to the previous 212 N, has generally been required to achieve fracture (Table 9). For either configuration, the point most susceptible to reach the failure was located at the scaphoid waist.

Thirdly, for the set *boundary conditions III*, the fracture is reached when the force is five times the one of the study (Table 10). Moreover, it is located in the proximal part of the bone, but on the side opposite to the joint zone with the radius, that is, in the proximal part closest to the lunate.

Fourthly, in order to achieve breakage for set *boundary conditions IV*, considerably large forces must be applied (Table 11). The waist is, again, the most fragile area of the bone. Specifically, the part of the waist that would break first is the part bordering the large bone. As well as in sets I, II, III and IV, the ulnar abduction is the movement most prone to reach the failure since it needs a lower applied load. For sets II and IV, the flexion requires the largest amount of load to break, contrary to what happened with set I, where it was the easiest mechanism of failure.

Table 12
Fracture criteria with 212 N load and contact between bones (I).

Movement	Direction	FR	Hoffman	Cowin
Flexion	+Y	1.53	1.97	0.48
Extension	−Y	1.52	3.41	0.44
Radial abduction	+X	0.56	0.8	0.3
Ulnar abduction	−X	0.55	0.78	0.42

Table 13
Fracture criteria with 212 N load and contact between bones (II).

Movement	Direction	FR	Hoffman	Cowin
Flexion	+Y	1.54	1.97	0.48
Extension	−Y	1.52	3.4	0.44
Radial abduction	+X	0.55	0.69	0.28
Ulnar abduction	−X	0.55	0.78	0.42

Table 14
Fracture criteria with 212 N load and contact between bones (III).

Movement	Direction	FR	Hoffman	Cowin
Flexion	+Y	1.53	1.05	0.4
Extension	−Y	1.51	3.41	0.35
Radial abduction	+X	0.31	0.8	0.31
Ulnar abduction	−X	0.55	0.78	0.42

3.2. Contact between bones

Since within the first approximation the mechanical context of the bone has been successfully reproduced, the aim of this second approach is to adjust to a real context in which there is no interaction between adjacent bones if there is separation with them. Thus, a set of simulations have been carried out on a model in which, apart from the scaphoid, the contact surfaces with the neighboring bones have been included.

In this model, the same elastic constants have been used to define the mechanical behavior of the bone. As boundary conditions, a fixation has been imposed in the area of the scaphoid that articulates with the radius. In addition, the employment of contact mechanics has been incorporated in the regions encompassing the large and lunate bones. A force of 212 N was uniformly applied across all 100 nodes constituting the adjacent area of the trapezium. Consistent with prior simulations, the force was applied to replicate the four movements of the hand as per the reference coordinate system illustrated in Fig. 7.

In this first case, the large bone is considered as a contact surface (*Contact I*). About the results, the force of 212 N is enough to cause the scaphoid fracture if applied in any direction of the Y direction, i.e., both in flexion and extension (see Table 12). The rest of the values are comparable to those of the Table 4.

Secondly, when utilizing the lunate contact surface (*Contact II*), the computational model exhibits a behavior that closely resembles that of the previous case (refer to Table 13). The obtained values for the fracture criteria in all configurations demonstrate a high degree of similarity, indicating that the stress–strain states in both scenarios are also highly comparable.

Finally, with the contacts with the lunate and capitate (*Contact III*), the behavior is also very similar to the two previous cases, except in radial abduction, where the fracture risk value is slightly lower (Table 14). We can conclude that this set of simulations is the most trustable one, since employs all the possible contacts. As all the results are comparable, this lower value of the fracture risk in radial abduction shows that with both contacts the bending of the scaphoid is more restricted, what is realistic.

Analyzing the results within the model with contact surfaces, in any of the cases and configurations, a force of 212 N has a greater impact on scaphoid fracture. Specifically, this force is sufficient to cause fracture in flexion and extension for any configuration (Tables 12–14).

Table 15
Elements and mesh sizes of the meshes employed in the mesh sensitivity study.

	Elements	Average Mesh size [mm]
H0	15083	3.2
H1	23535	2.7
H2	35031	2.4
H3	59565	2.0
H4	97342	1.7

Moreover, under the presence of contacts, the only area susceptible to break is the proximal pole. In fact, failure tends to occur in the part closest to the radius.

The behavior of the simulations with contacts resembles the first case of the simulations without contacts, where the scaphoid has been fixed only in its articulation zone with the radius and has been left free in the rest of the joints. In all these cases, the fracture is reached in flexion and extension, that is, when applied in either direction of the Y axis of the reference system. Likewise, in both models, the values of the fracture criteria are practically the same for all wrist movements, so it can be estimated that the stress–strain configuration is very similar.

In conclusion, to obtain a simplified model able to simulate the mechanical behavior of the scaphoid taking into account the contact with its neighboring bones, it is sufficient to use a model consisting of the bone and impose the fixation in the area that articulates with the radius and apply a force in the region of union with the trapezium. Therefore, a mechanical problem with contacts can be solved by means of a model based solely on boundary conditions. In this way, through this method, the results of more advanced calculations could be estimated through much simpler ones, thus allowing a saving in computational cost.

3.3. Mesh sensitivity analysis

In order to verify the suitability of the employed mesh within the modeled problem, a study of the results of fracture criterion depending on the mesh size has been carried out. The proposed model is the one with the 2 contact surfaces for capitate and lunate bones (case: contact between bones (III)). The Hoffman criterion has been employed within this study, since we have chosen this one as the reference for the scaphoid fracture study. In Table 15 we can see the 5 employed meshes. The loads are the ones employed on the analysis depicted in Table 8, the ones that give a fracture criterion equal to 1.

In Fig. 10, the results of the Hoffman criterion are depicted for the 4 studied movements, as well as an average of these 4 results. We can observe that, as mesh refinement increases, the average line progressively converges to a fracture risk value of 1. This observation indicates a convergence of results with finer mesh resolutions. Beginning with mesh H3 (average mesh size 2.0 mm), we can assert that the quality of the mesh is satisfactory for addressing the specific problem under consideration. The mesh considered in our modeling, for which the results are reported in Sections 3.1 and 3.2, has an average mesh size of 1.85 mm. Thus, this mesh configuration is well-suited for our purposes. Nonetheless, employing coarser meshes could enhance computational efficiency. It is important to note, however, that this is not a primary concern when dealing with pre-failure elastic problems.

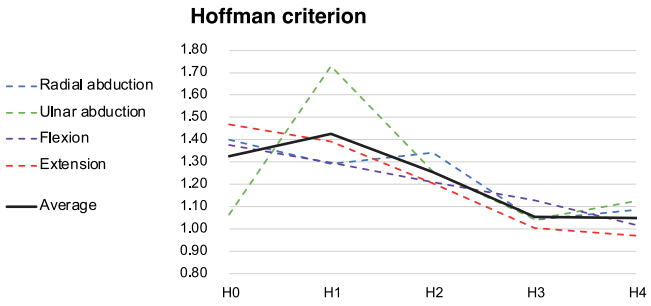

Fig. 10. Hoffman fracture results for the 5 different employed meshes.

4. Discussion and conclusions

In this paper, the study of scaphoid fractures was conducted using a model derived from real CT image of the wrist. The investigation was approached using two different simulation set ups: the first utilizing Dirichlet boundary conditions, and the second employing surface contact-type interactions.

In the first simulation set up, which solely incorporated boundary conditions, fracture occurred at significantly high force magnitudes. Furthermore, the fracture manifested in two distinct regions of the scaphoid: the proximal pole and the waist. Regarding the location of the fracture, a clear pattern dependent on the boundary conditions has been observed. Interestingly, this pattern remained consistent regardless of the forces induced by various wrist movements, indicating that the fracture location was independent of the direction and magnitude of the applied forces.

In the second simulation set up that also incorporated surface contact interactions, it has been observed that breakage occurs for lower force values. In particular, it was found that a force magnitude of 212 N applied in the Y-axis was sufficient to induce bone fracture regardless of the type of contact. For all cases, the fracture has taken place in the part of the proximal pole near the radius.

Moreover, it was observed that the scaphoid model, when subjected to boundary conditions BC I (see Table 3), where the capitate and lunate bones are allowed to move freely, exhibited similar behavior to any model incorporating contact interfaces. This finding implies that fixing the interaction areas with the lunate and capitate bones produces erroneous outcomes, as it restricts the realistic bending of the scaphoid. Therefore, it is more accurate to utilize contact interfaces in these regions, or alternatively, if computational costs need to be minimized, to leave them unconstrained.

Fracture was studied using three criteria: fracture risk (from von-Mises), Hoffman and Cowin. Thus, fracture occurrence was established when at least one of the elements of the model reached a value equal to or greater than unity according to each criterion. It is important to note that there is no one-size-fits-all criterion for analyzing bone tissue, and the best choice should be based on the specific requirements and characteristics of the analysis. Researchers often use a criterion that aligns with the material properties and loading conditions of interest, while considering the trade-offs between simplicity and accuracy in their modeling approach. In our case, for the available data and problem conditions, Hoffman's criterion has resulted as the best choice. This is why we have employed this methodology for the mesh sensitivity analysis.

Following, some considerations for why the Hoffman criterion might be preferred over Cowin's or von-Mises for this problem are provided:

- Strength Asymmetry in Bone: Bone tissue exhibits strength asymmetry, meaning it has different strengths in tension and compression. The Hoffman criterion accounts for this by considering the difference between tension and compression, making it more suitable for modeling bone's behavior under various loading conditions than others such as von-Mises one.
- Behavior in All Directions: The Hoffman criterion considers the material's behavior in all directions, which can be important for bone tissue, as bones are not isotropic; their structural properties can vary in different directions due to their microstructure.
- Simplicity: While Cowin's or Tsai–Wu criteria may offer more detailed insights into the behavior of complex materials, the

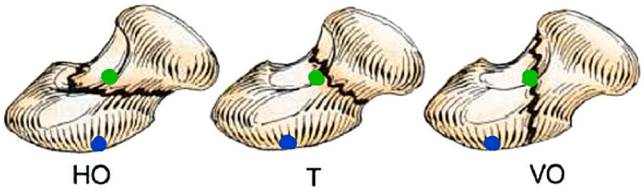

Fig. 11. Relationship between fracture initiation point and Rüsse classification (Moreno, 2013).

Hoffman criterion is relatively simpler and more straightforward to implement. In practical engineering and medical applications, simplicity can be an advantage. It is true that Cowin's criterion employed within this research is a simplified model, but the obtained results are far from the other 2 methodologies.

- Applicability: The choice of criterion also depends on the specific goals of the analysis. If the primary goal is to assess bone fracture risk or predict the behavior of bone under various loading conditions, the Hoffman criterion's focus on strength asymmetry and multidirectional behavior may be sufficient and practical.
- Experimental Validation: The choice of criterion can also be influenced by the availability of experimental data and validation studies, which is not the case in this research. Thus, Hoffman's criterion provides a general framework for the study without necessity of experiments.

Although it is challenging to directly compare these results with experimental tests to assess the accuracy of the methods, our study can infer the initiation point of fractures.

The two identified fracture patterns in our study can be associated with different types of fractures based on their location. In particular, they can be related to Rüsse's classification (Vázquez, 2007).

Fig. 11 shows the three types of fractures according to Rüsse, together with the initiation points that have been found. The blue point represents the point of initiation of the break at the proximal pole, while the green point represents the point of initiation at the waist. As can be seen, the point located at the waist is located very close to the trajectory of all fracture types. However, the initiation point on the proximal pole only approximates the crack that occurs in vertical oblique (VO) fractures. In particular, it can be estimated that these fractures occur when there are simultaneously two elements under high stresses at the marked points.

Certainly, there is no sufficient data to draw definitive conclusions regarding the direction of crack propagation. A full analysis that incorporates explicit crack propagation is needed to accurately determine the direction of crack growth.

The main limitations of the proposed research are:

- No explicit fracture, as mentioned in the previous paragraphs.
- Only the deformation of the scaphoid is considered, taking the rest of the bones as rigid bodies.
- Isotropic materials.
- Homogeneous materials. With the current image resolution, the results do not show a discernible segmentation pattern within cortical and trabecular bones, which can be used to generate non-homogeneous meshes.

The goal of future developments following the lines of the present study will be the assessment of the stabilization of fractures through different techniques such as 3D-printing, similar to the one made by Lu et al. with the fracture of the ankle (Lu et al., 2021), employing the FEA prior to the real stabilization in order to reproduce possible complexities that may appear. The addition of crack propagation would help to see how a stabilization technique could relax the crack propagation.

CRediT authorship contribution statement

Ana B. Maroto: Validation, Software, Methodology, Investigation, Formal analysis, Conceptualization. **Pedro Navas:** Writing – original draft, Resources, Methodology, Formal analysis, Conceptualization. **Felicia Alfano:** Writing – original draft, Visualization, Software, Conceptualization.

Declaration of competing interest

The authors declare the following financial interests/personal relationships which may be considered as potential competing interests: Pedro Navas reports financial support, administrative support, and article publishing charges were provided by Polytechnic University of Madrid. Felicia Alfano reports financial support and administrative support were provided by Polytechnic University of Madrid.

Data availability

The authors do not have permission to share data.

Acknowledgments

We would like to thank the administrative support of Universidad Politécnica de Madrid. Also, the advices provided by Prof. José M. Goicolea have been greatly appreciated.

References

Anderson, D.D., Deshpande, B.R., Daniel, T.E., Baratz, M.E., 2005. A three-dimensional finite element model of the radiocarpal joint. Iowa Orthopaedic J. 25, 108–117, URL https://www.ncbi.nlm.nih.gov/pmc/articles/PMC1888764/.

Bajuri, M., Kadir, M.R.A., Raman, M.M., Kamarul, T., 2012. Mechanical and functional assessment of the wrist affected by rheumatoid arthritis: A finite element analysis. Med. Eng. Phys. 34 (9), 1294–1302. http://dx.doi.org/10.1016/j.medengphy.2011.12.020.

Caeiro, J., González, P., Guede, D., 2013. Biomechanics and bone (& II): Trials in different hierarchical levels of bone and alternative tools for the determination of bone strength. J. Osteoporos. Miner. Metabol. 5 (2).

Cody, D.D., Gross, G.J., Hou, F.J., Spencer, H.J., Goldstein, S.A., Fyhrie, D.P., 1999. Femoral strength is better predicted by finite element models than QCT and DXA. J. Biomech. 32, 1013–1020. http://dx.doi.org/10.1016/s0021-9290(99)00099-8.

Cowin, S.C., 1986. Fabric dependence of an anisotropic strength criterion. Mech. Mater. 5 (3), 251–260. http://dx.doi.org/10.1016/0167-6636(86)90022-0.

Cristofolini, L., Schileo, E., Juszczyk, M., Taddei, F., Martelli, S., Viceconti, M., 2010. Mechanical testing of bones: The positive synergy of finite element models and in vitro experiments. Phil. Trans. R. Soc. A 368 (1920), 2725–2763. http://dx.doi.org/10.1098/rsta.2010.0046.

de Souza Neto, E.A., Owen, D.R.J., Perić, D., 2008. Computational Methods for Plasticity. John Wiley & Sons Ltd., The Atrium, Southern Gate, Chichester, UK, http://dx.doi.org/10.1002/9780470694626.

Doblaré, M., Gómez-Benito, M.J., García-Aznar, J.M., 2004. Modelling bone tissue fracture and healing: A review. Eng. Fract. Mech. 71, 1809–1840. http://dx.doi.org/10.1016/j.engfracmech.2003.08.003.

Enns-Bray, W., Ariza, O., Gilchrist, S., Widmer Soyka, R., Vogt, P., Palsson, H., Boyd, S., Guy, P., Cripton, P., Ferguson, S., Helgason, B., 2016. Morphology based anisotropic finite element models of the proximal femur validated with experimental data. Med. Eng. Phys. 38 (11), 1339–1347. http://dx.doi.org/10.1016/j.medengphy.2016.08.010.

Erhart, J., Unger, E., Schefzig, F., Varga, P., Hagman, M., Ristl, R., Hajdú, S., Gormasz, A., Sadoghi, P., Mayr, Y., 2020. Wrist movements induce torque and lever force in the scaphoid: An ex vivo study. J. Orthop. Surg. Res. 15, http://dx.doi.org/10.1186/s13018-020-01897-y.

Falcinelli, C., Schileo, E., Pakdel, A., Whyne, C., Cristofolini, L., Taddei, F., 2016. Can CT image deblurring improve finite element predictions at the proximal femur? J. Mech. Behav. Biomed. Mater. 63, 337–351. http://dx.doi.org/10.1016/j.jmbbm.2016.07.004.

Fang, Q., 2002, iso2mesh: A 3D surface and volumetric mesh generator for MATLAB/Octave, URL https://es.mathworks.com/solutions/medical-devices/medical-imaging.html.

Fenech, C.M., Keaveny, T., 1999. A cellular solid criterion for predicting the axial-shear failure properties of bovine trabecular bone. J. Biomech. Eng. 113, 414–422. http://dx.doi.org/10.1115/1.2798339.

Frank, P., Von Mises, R., 1961. Die Differential-und Integralgleichungen der Mechanik und Physik. Braunschweig, Vieweg.

Gómez-Benito, M.J., Fornells, P., Garcí a Aznar, J.M., Seral, B., Seral-Iñnigo, F., Doblaré, M., 2007. Computational comparison of reamed versus unreamed intramedullary tibial nails. J. Orthopaedic Res. 25 (2), 191–200. http://dx.doi.org/10.1002/jor.20308.

Helgason, B., Viceconti, M., Rúnarsson, T.P., Brynjólfsson, S., 2008. On the mechanical stability of porous coated press fit titanium implants: A finite element study of a pushout test. J. Biomech. 41 (8), 1675–1681. http://dx.doi.org/10.1016/j.jbiomech.2008.03.007.

Hoffman, O., 1967. The brittle strength of orthotropic materials. J. Compos. Mater. 1 (2), 200–206. http://dx.doi.org/10.1177/002199836700100210.

Keaveny, T., Wachtel, E., Zadesky, S., Arramon, Y., 1999. Application of the Tsai–Wu quadratic multiaxial failure criterion to bovine trabecular bone. J. Biomech. Eng. 121, 99–107. http://dx.doi.org/10.1115/1.2798051.

Keyak, J., Rossi, S., 1983. Prediction of femoral fracture load using finite elements models: An examination of stress and strain-based failure theories.. J. Biomech. 33, 209–214.

Keyak, J., Rossi, S., Jones, K., Les, C., Skinner, H., 2001. Prediction of fracture location in the proximal femur using finite element models. Med. Eng. Phys. 23 (9), 657–664. http://dx.doi.org/10.1016/S1350-4533(01)00094-7.

Keyak, J., Sigurdsson, S., Karlsdottir, G., Oskarsdottir, D., Sigmarsdottir, A., Kornak, J., Harris, T., Sigurdsson, G., Jonsson, B., Siggeirsdottir, K., Eiriksdottir, G., Gudnason, V., Lang, T., 2013. Effect of finite element model loading condition on fracture risk assessment in men and women: The AGES-Reykjavik study. Bone 57 (1), 18–29. http://dx.doi.org/10.1016/j.bone.2013.07.028.

Lotz, J., Cheal, E., W.C., W.H., 1991. Fracture prediction for the proximal femur using finite element models: Part I—-Linear analysis. J. Biomech. 113, 353–360.

Lu, P., Liao, Z., Zeng, Q., Chen, H., Huang, W., Liu, Z., Chen, Y., Zhong, J., Huang, G., 2021. Customized three-dimensional-printed orthopedic close contact casts for the treatment of stable ankle fractures: Finite element analysis and a pilot study. ACS Omega 6 (4), 3418–3426. http://dx.doi.org/10.1021/acsomega.0c06031.

Luria, S., Hoch, S., Liebergall, M., Mosheiff, R., Peleg, E., 2010. Optimal fixation of acute scaphoid fractures: Finite element analysis. J. Hand Surg. 35 (8), 1246–1250. http://dx.doi.org/10.1016/j.jhsa.2010.05.011.

Malmeister, A.K., 1966. Geometry of theories of strength. Polym. Mech. 2 (4), 324–331. http://dx.doi.org/10.1007/BF00860067.

Moreno, C., 2013. Fracturas del escafoides. URL https://es.slideshare.net/christianmoreno35/fracturas-del-escafoides-42617262.

Oliva, J., 2007. Modelos de cálculo para solicitaciones estáticas y dinámicas en huesos. Aplicación a la simulación mediante elementos finitos de impactos en el fémur humano. 102–109, ETSI Caminos, Canales y Puertos, UPM, Madrid, URL https://core.ac.uk/download/pdf/148654217.pdf.

Rothenfluh, E., Jain, S., Guggenberger, R., Taylor, W.R., Nasab, S.H.H., 2023. The influence of partial union on the mechanical strength of scaphoid fractures: A finite element study. J. Hand Surg. (Eur. Vol.) 17531934231157565. http://dx.doi.org/10.1177/17531934231157565.

Schileo, E., Dall'Ara, E., Taddei, F., Malandrino, A., Schotkamp, T., Baleani, M., Viceconti, M., 2008. An accurate estimation of bone density improves the accuracy of subject-specific finite element models. J. Biomech. 41 (11), 2483–2491. http://dx.doi.org/10.1016/j.jbiomech.2008.05.017.

Slutsky, D., Slade, J., 2011. The Scaphoid. In: Thieme Publishers Series, Thieme.

Tortora, G., Derrickson, B., 2018. Principles of Anatomy and Physiology. Wiley.

Tsai, S.W., Wu, E.M., 1971. A general theory of strength for anisotropic materials. J. Compos. Mater. 5 (1), 58–80. http://dx.doi.org/10.1177/002199837100500106.

Varga, P., Schefzig, P., Unger, E., Mayr, W., Zysset, P.K., Erhart, J., 2013. Finite element based estimation of contact areas and pressures of the human scaphoid in various functional positions of the hand. J. Biomech. 46 (5), 984–990. http://dx.doi.org/10.1016/j.jbiomech.2012.11.053.

Varga, P., Zysset, P.K., Schefzig, P., Unger, E., Mayr, W., Erhart, J., 2016. A finite element analysis of two novel screw designs for scaphoid waist fractures. Med. Eng. Phys. 38 (2), 131–139. http://dx.doi.org/10.1016/j.medengphy.2015.11.006.

Vázquez, J.M.F., 2007. Clasificación de las fracturas de escafoides. Artemisa en línea 3 (4), 238–243, URL https://www.medigraphic.com/pdfs/orthotips/ot-2007/ot074g.pdf.

Villalobos, I.P., 2007. Finite element study of proximal carpectomy of a wrist. URL https://upcommons.upc.edu/handle/2099.1/4563.

Yeh, H.-Y., Murphy, H.C., Yeh, H.-L., 2009. An investigation of failure criterion for new orthotropic ceramic matrix composite materials. J. Reinf. Plast. Compos. 28 (4), 441–459. http://dx.doi.org/10.1177/0731684407085429.